Operational Topic

An evaluation of a counting system that can serve as an in-field, high-resolution whole body counter for fission and activation products.

The HML's New Field Deployable, High-Resolution Whole Body Counter

*Gary H. Kramer, Kevin Capello, and Barry M. Hauck**

Abstract: *The Human Monitoring Laboratory has found an alternate use for a hyperpure germanium field deployable instrument that was originally designed to be used in a search and identify mode for contraband radioactive material. The instrument, the Ortec Detective, becomes a fully functional spectroscopy system when connected to a laptop computer. In this configuration it can be used as a high-resolution portable whole body counter. This work has determined that the instrument has adequate sensitivity for emergency response with respect to fission and activation products, but not actinides. The use of Monte Carlo simulations has allowed the HML to calibrate the instrument, partially optimize the counting geometry, and develop a calibration curve that is a function of photon energy and a persons' size. Similarly for thyroid counting, a function has been found that fits counting efficiency to a person's height. The MDA's are a few kilo Becquerels for fission and activation products for a 5-min count in an unshielded environment using a male subject. Health Phys. 89(Supplement 5):S60–S68; 2005*

Key words: *operational topic; whole body counting; radiological terrorism; counting efficiency*

INTRODUCTION

Prior to the tragic events of 11 September 2001, the Human Monitoring Laboratory's (HML) contribution to the Federal Nuclear Emergency Plan, which is operated by the Health Canada's Nuclear Emergency Preparedness and Response Division, was staff and expertise to the Technical Advisory Group, and occasionally providing a staff member to act as an On-Call Duty Officer. After the World Trade Center was destroyed, ripples of anti-terrorist activities spread around the world. The Government of Canada was no exception to this response and initiated a three-phase response.

Health Canada, along with other government departments that might have a stake in fighting terrorism, was tasked with filling gaps identified in an internal risk analysis. An initiative was rapidly set up that allocated $170 million (CAN) to a three-phase five-year plan. It was put into place by early 2002. The three phases were: Technology Acquisition (must be between two or more Federal Government departments), Technology Acceleration (must include one or more Federal Government department and an industrial partner), and Research and Development (must include one or more Federal Government department and another partner, e.g., university).

The risk analysis mentioned above identified many nuclear and radiological scenarios, most of which could result in internal contamination. The numbers of potentially affected people varied from a few persons to large groups. The HML proposed several solutions to help fill some of the identified gaps, and three proposals were accepted. The details of this initiative have been published elsewhere (Kramer 2004).

This paper describes an alternate use for one of instruments acquired under this initiative: the Ortec Detective (Ortec, 801 South Illinois Avenue, Oak Ridge, TN 37830). This instrument is a HPGe detector cooled by miniature, high-reliability mechanical cooler that can operate from battery, line power, or from 12 V DC. It is designed to provide a rapid, simple, and reliable classification of naturally occurring radioactive materials (NORM), medical isotopes, industrial isotopes, and nuclear isotopes. It is limited to search and identify modes (including dose rate) when operated in a stand-alone mode; however, when connected to a laptop computer, it becomes a fully functional spectroscopy system.

* *Human Monitoring Laboratory, Radiation Surveillance and Heath Assessment Division, Radiation Protection Bureau, 775 Brookfield Road, PL6302D1, Ottawa, Ontario, K1A 1C1, Canada.*

Gary H. Kramer completed his Ph.D. in the School of Molecular Sciences, University of Sussex, U.K., in 1975, where he was studying solution kinetics. He moved to Canada to take a postdoctoral position at the University of Calgary and then to the University of Toronto for four years. In 1979, he joined Atomic Energy of Canada Limited and worked on bioassay methods development. He transferred to Health Canada in 1987 and became the Head of the Human Monitoring Laboratory. He has been actively involved in research in the field of In Vivo monitoring since that time. His email is gary_h_kramer@hc-sc.gc.ca.

The Human Monitoring Laboratory (HML), which operates the Canadian National Calibration Reference Centre for In vivo Monitoring (Kramer and Limson Zamora 1994), has extended the use of the Detective to that of an emergency high resolution portable whole body counter that can be used in the field following a terrorist attack or other incident releasing radioactive material.

The anticipated use of this instrument will be in conjunction with the four portal monitors that the HML can field-deploy to screen up to 1,000 persons per hour. The sensitivity of the portal monitors is such that they will alarm if a person contaminated with approximately 60 kBq of a fission/activation product (e.g., 0.4 mSv committed effective dose for ^{137}Cs) pauses for a 2-s delay between the detectors. Any person alarming the monitors would first go through a decontamination procedure and than be recounted to confirm the result. If the recount still alarms the portal monitors, the contaminated person would be referred to the field team using the portable whole body counter for further follow-up.

The design criteria for the field-deployable whole body counter is that it should be portable; high resolution (thus able to identify a complex mixture of radionuclides); not dependent on liquid nitrogen for cooling; the accuracy of the in vivo measurement should identify persons at immediate, intermediate, and minimal health risk; and only persons containing 60 kBq or more are likely to be monitored. This paper describes an instrument whose characteristics meet these requirements, its calibration, and its sensitivity.

MATERIALS AND METHODS

The Ortec Detective

The Detective was acquired from Ametek's Ortec division (Ametek, Ortec Division, 801 South Illinois Avenue, Oak Ridge, TN 37831-0895). It is shown in Fig. 1. The Detective's portable nuclide identifier (based on gamma-ray emissions only) provides the following functions: search (scanning mode for location of radioactive sources, with audio alert using an external earpiece); identify (proprietary scheme for identification and classification of radionuclides); and dose rate (gamma dose rate is monitored by an internal compensated GM tube).

Typical identifications are:

- Industrial—including but not limited to ^{57}Co, ^{60}Co, ^{133}Ba, ^{137}Cs, ^{192}Ir, ^{241}Am, ^{75}Se;
- Medical—including but not limited to ^{18}F, ^{67}Ga, ^{99m}Tc, ^{111}1n, ^{123}1, ^{131}1, ^{133}Xe, ^{201}T1;
- NORM—including but not limited to ^{40}K, ^{226}Ra, ^{232}Th, ^{238}U; and
- Nuclear—including but not limited to ^{233}U, ^{235}U, ^{237}Np, ^{239}Pu, ^{252}Cf.

These classifications are based on internal, fixed library that cannot (at the present time) be changed by the user.

When the Detective is connected to a laptop computer running Ortec's Renaissance software, it becomes a fully functional spectroscopy system that could be used as a resolution whole body counter.

Figure 1. The Ortec Detective standing on the charging bay.

Calibration

The Detective was calibrated for whole body counting using Monte Carlo simulations. The design of the Detective is proprietary, and only limited formation about the configuration within the end cap could be obtained from the manufacturer, making the Monte Carlo modeling more challenging than usual.

The modeling of the Bottle Manikin Absorber (BOMAB) phantoms has been described elsewhere (Kramer et al. 2002). Each member of the HML's BOMAB phantom family (Kramer et al. 1991) was used in the simulations: 95-percentile male, reference male, reference female, 5-percentile male, 10-y-old, and 4-y-old. The walls of the BOMAB phantom were high density (0.95 g cm^{-3}) polyethylene and the interior sections were filled with water. These interior sections were defined in the simulations as the sources with emission probabilities being proportional to the volumes of the sections (i.e., the material is homogeneously distributed throughout the phantom). Two counting geometries were simulated (see Fig. 2). First, the detector was fixed in space 100 cm above the ground plane and 50 cm from the front surface of a standing phantom placed vertically in front of the Detective to simulate a person standing in front of the Detective that would be placed on a table. This will be known as counting geometry 1 hereafter. The second geometry is similar to counting

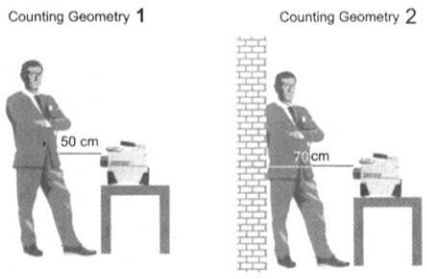

Figure 2. Schematic diagram of counting geometry 1 and counting geometry 2.

geometry 1, except the phantoms were placed with their back against a wall that was 70 cm from the Detective. This counting geometry simulates that of instruments like the Canberra FastScan. This will be known as counting geometry 2 hereafter. In both counting geometries 1 and 2, the reference male phantom is in the same position relative to the detector.

Simulations—whole body counting. The Monte Carlo code used for the simulations was MCNP5 (Monte Carlo N-Particle), which is described elsewhere (X-5 Monte Carlo Team 2003) and was obtained from the Radiation Safety Information Computational Center (Post Office Box 2008, 1 Bethel Valley Road, Oak Ridge, TN 37831-6171). MrCNP5 is a general-purpose program that can be used for neutron, photon, electron, or coupled neutron/photon/electron transport, although this work makes use of the photon transport capabilities. It has been used for many applications, such as radiation protection and dosimetry, radiation shielding radiography, medical physics, nuclear criticality safety, detector design and analysis, nuclear oil well logging, etc.

The authors of MCNP consider that a relative error on a predicted value calculated by the code of 0.1–0.2 suggests that the tally result is questionable (X5 Monte Carlo Team 2003). Tally results for which the relative error is above 0.2 are not likely to be meaningful; however, results are generally reliable for a relative error less than 0.1.

The source was defined as the inner sections of the phantom that correspond to the cavities that would be filled with radioactive solution for a real phantom. The emission probabilities were set proportional to the volumes of the sections. The following energies were simulated individually: 40, 60, 120, 240, 344, 660, 898, 1000, 1173, 1332, and 1836 keV. Many of these energies will be recognized for being close to the primary energy of common radionuclides (e.g., 662 keV ^{137}Cs), and other energies were used to fill in the calibration curve. Ten million photons were generated and those that reached the detector and deposited full energy therein were tallied (tally type f8). Relative errors for all tally results were less than 0.099 for all simulations.

Simulations—point sources. The disc source experiments described below were reproduced by Monte Carlo simulations. Each disc was simulated as a short cylinder of polyethylene of the same dimensions as the physical sources with a point source in the center of the disc. Energies simulated were 60, 81, 276, 303, 356, 383, 662, and 1173 keV. Each run was mono-energetic and 10^7 photons were run for each simulation. Relative errors for all tally results were less than 0.082 for all simulations

Simulations—thyroid counting. The localization of ^{131}I in the thyroid was simulated by placing a virtual thyroid gland in the neck of each phantom; the glands were sized appropriately to each phantom (ICRP 2002). The effect of gland size was also investigated by placing different sized thyroids in the reference male phantom (Pankow et al. 1985). Table 1 summarizes the sizes used in all of the trials. Photons (365 keV) were emitted as if coming from a homogeneously distributed source within the thyroid. All other conditions of the model described above were maintained for both counting geometries. Relative errors for all tally results were less than 0.061 for all simulations.

Table 1. Sizes of thyroid glands simulated for the different phantoms and also the different sizes used with the PM phantom.

Phantom	Mass (g)	Trial Number	Mass (g)
P4	3.2	1	11
P10	9.6	2	14
PM5	16.9	3	17.2
PF	16.9	4	20.6
PM	20	5	22.7
PM95	25.8	6	26.8
		7	29.1

P4 = four-y-old, P10 = ten-y-old, PM5 = five-percentile male, PF = reference female, PM = reference male, PM95 = 95-percentile male.

Experimental counts

Background. The Detective measured an unshielded ambient background in the HML for 3,600 s. The resulting spectrum was used to determine MDA values as described below.

Disc sources. Four disc sources (^{137}Cs, ^{60}Co, ^{133}Ba, and ^{241}Am) were measured with the Detective. Each source was fixed to the rear wall of the HML's whole body counting chamber so that the detector source distance was 50 cm and the source and detector crystal centers were horizontal. Depending on the activity of the disc source (2–37 kBq), the counting time varied from 20,000 to 50,000 s.

Phantom count. A BOMAB male phantom was measured for 3,600 s in counting geometry 2 to obtain sufficient counts to determine experimental counting efficiencies. The phantom contained 7.5 kBq ^{137}Cs, 7.4 kBq ^{60}Co, and 6.6 kBq ^{57}Co (3 May 2005). The experimental counting efficiencies of the 122 keV, 662 keV, 1173 keV, and 1333 keV photopeaks were determined from the net counts.

Minimum detectable activity (MDA)

The unshielded background mentioned above is assumed to be that of a person standing in front of the Detective in either counting geometry. The counts for the photopeaks of interest (^{137}Cs, ^{60}Co, ^{152}Eu, and ^{7A1}Am) were taken from the same regions of interest that were used in the calibrations described above.

The following formula for MDA is based on the work of Currie (1968), with Brodsky's (1986) modification, although in practice, and in this work, the second term is neglected as it adds little to the magnitude of the result when N is large:

$$MDA = \frac{4.65\sqrt{N}}{ET} + \frac{3}{ET}, \quad (1)$$

where N = background counts in the region of interest, E = counting efficiency (cps Bq^{-1}), and T = counting time (s).

Dosimetric implications

Calculations of intakes and dose were performed using Integrated Modules for Bioassay Analysis (IMBA) Professional CANDU-Edition (Phases I & II) provided by ACJ & Associates, Inc (129 Patton Street, Richland, WA 99352-1618). Other data manipulations were performed using Microsoft Excel. Regression analyses were performed with Table Curve 2D and Table Curve 3D (SPSS Inc., 444 N Michigan Avenue, Chicago, IL 60611).

Table 2. Counting efficiencies of the phantoms as a function of energy for counting geometry 1

Phantom	Energy (keV)	Eff (cnt/photon)	Phantom	Energy (keV)	Eff (cnt/photon)
P4	40	1.00×10^{-5}	PF	40	9.35×10^{-6}
	60	3.06×10^{-5}		60	2.91×10^{-5}
	120	7.14×10^{-5}		120	6.76×10^{-5}
	240	5.49×10^{-5}		240	5.06×10^{-5}
	344	4.17×10^{-5}		344	3.58×10^{-5}
	660	2.24×10^{-5}		660	1.74×10^{-5}
	898	1.79×10^{-5}		898	1.53×10^{-5}
	1,000	1.66×10^{-5}		1,000	1.40×10^{-5}
	1,173	1.60×10^{-5}		1,173	1.09×10^{-5}
	1,332	1.52×10^{-5}		1,332	9.78×10^{-6}
	1,836	1.19×10^{-5}		1,836	9.86×10^{-6}
	40	1.04×10^{-5}	PM	40	7.70×10^{-6}
	60	3.19×10^{-5}		60	2.63×10^{-5}
	120	7.63×10^{-5}		120	6.03×10^{-5}
	240	5.58×10^{-5}		240	4.36×10^{-5}
	344	3.77×10^{-5}		344	3.13×10^{-5}
	660	2.32×10^{-5}		660	1.86×10^{-5}
	898	1.60×10^{-5}		898	1.42×10^{-5}
	1,000	1.58×10^{-5}		1,000	1.35×10^{-5}
	1,173	1.32×10^{-5}		1,173	1.22×10^{-5}
	1,332	1.17×10^{-5}		1,332	1.12×10^{-5}
	1,836	8.99×10^{-6}		1,836	8.13×10^{-6}
	40	9.21×10^{-6}	PM95	40	5.04×10^{-6}
	60	2.86×10^{-5}		60	1.89×10^{-5}
	120	7.07×10^{-5}		120	4.03×10^{-5}
	240	5.20×10^{-5}		240	3.06×10^{-5}
	344	3.85×10^{-5}		344	2.29×10^{-5}
	660	2.13×10^{-5}		660	1.28×10^{-5}
	898	1.81×10^{-5}		898	1.10×10^{-5}
	1,000	1.61×10^{-5}		1,000	1.06×10^{-5}
	1,173	1.29×10^{-5}		1,173	9.57×10^{-6}
	1,332	1.18×10^{-5}		1,332	9.06×10^{-6}
	1,836	1.07×10^{-5}		1,836	6.04×10^{-6}

P4 = four-y-old, P10 = ten-y-old, PM5 = five-percentile male, PF = reference female, PM = reference male, PM95 = 95-percentile male.

RESULTS AND DISCUSSION

Calibration—whole body counting

The counting efficiencies of the phantoms as a function of photon energy are shown in Tables 2 and 3. These values have been adjusted for the empirical parameter (1.39) that was developed above. This parameter takes into account the approximations made by the Monte Carlo model compared with the real equipment (Mallett et al. 1995; RSICC 1997).

Previous work (Smith et al. 1979) found that the counting efficiency of a whole body counter was proportional to (weight/height)$^{1/2}$. Fig. 3 shows the efficiency plotted against this size parameter for counting geometry 1 for different photon energies. It seems reasonable that there should also be an expression that will fit the size parameter and photon energy to the counting efficiency. The following expression has been found to give a good fit to the data and is related to other functions found by the HML (Kramer and Capello 2004):

$$Ln(Z) = a + bY^2 + \left(\frac{c + dY^2}{Ln(X)}\right) + \left(\frac{e + fY^2}{Ln(X)^2}\right) + \left(\frac{g + iY^2}{Ln(X)^3}\right) + \left(\frac{j + kY}{Ln(X)^4}\right), \quad (2)$$

where Z = counting efficiency, Y = weight/height, X = photon energy (keV), and a to k are regression coefficients.

Table Curve 3D was used to fit the data in Tables 2 and 3. For whole body counting using counting geometry 1 the correlation coefficient was 0.9906, the standard error of the fit was 0.0705, and the F-statistic of the fit was 656.6; Fig. 4 shows an example output of the fitted function with the data points. For whole body counting using counting geometry 2 the correlation coefficient was 0.9807, the standard error of the fit was 0.0907, and the F-statistic of the fit was 282.4.

Using eqn (2), the efficiency values in Table 2 can be predicted to within 18% (bias) and to within 14% (bias) for the data in Table 3. Table 2's range of bias values is from −12 to 18% with a mean of 0 ± 7%, and Table 3's

Table 3. Counting efficiencies of the phantoms as a function of energy for counting geometry 2

Phantom	Energy (keV)	Eff (cnt/photon)	Phantom	Energy (keV)	Eff (cnt/photon)
P4	40	9.35×10^{-6}	PF	40	8.71×10^{-6}
	60	2.55×10^{-5}		60	2.88×10^{-5}
	120	6.29×10^{-5}		120	6.50×10^{-5}
	240	4.67×10^{-5}		240	4.77×10^{-5}
	344	3.43×10^{-5}		344	3.40×10^{-5}
	662	1.94×10^{-5}		662	1.76×10^{-5}
	898	1.45×10^{-5}		898	1.43×10^{-5}
	1,000	1.34×10^{-5}		1,000	1.36×10^{-5}
	1,173	1.33×10^{-5}		1,173	1.09×10^{-5}
	1,332	1.26×10^{-5}		1,332	9.35×10^{-6}
	1,836	8.27×10^{-6}		1,836	9.50×10^{-6}
	40	9.78×10^{-6}	PM	40	7.70×10^{-6}
	60	3.01×10^{-5}		60	2.63×10^{-5}
	120	6.97×10^{-5}		120	6.03×10^{-5}
	240	5.20×10^{-5}		240	4.36×10^{-5}
	344	3.63×10^{-5}		344	0.00003
	662	2.09×10^{-5}		662	1.86×10^{-5}
	898	1.45×10^{-5}		898	1.43×10^{-5}
	1,000	1.32×10^{-5}		1,000	1.35×10^{-5}
	1,173	1.30×10^{-5}		1,173	1.22×10^{-5}
	1,332	1.17×10^{-5}		1,332	1.12×10^{-5}
	1,836	7.91×10^{-6}		1,836	8.13×10^{-6}
	40	8.42×10^{-6}	PM95	40	8.20×10^{-6}
	60	2.64×10^{-5}		60	2.40×10^{-5}
	120	6.35×10^{-5}		120	5.48×10^{-5}
	240	4.74×10^{-5}		240	4.14×10^{-5}
	344	3.55×10^{-5}		344	3.07×10^{-5}
	662	1.91×10^{-5}		662	1.68×10^{-5}
	898	1.58×10^{-5}		898	1.22×10^{-5}
	1,000	1.45×10^{-5}		1,000	1.16×10^{-5}
	1,173	1.18×10^{-5}		1,173	1.12×10^{-5}
	1,332	1.04×10^{-5}		1,332	1.09×10^{-5}
	1,836	8.99×10^{-6}		1,836	7.48×10^{-6}

P4 = four-y-old, P10 = ten-y-old, PM5 = five-percentile male, PF = reference female, PM = reference male, PM95 = 95-percentile male.

range of bias values is from −12 to 14% with a mean of 0 ± 6%.

The bias in this case is defined as:

$$Bias = \left(\frac{Calc - Observed}{Observed}\right), \qquad (3)$$

where *Calc* refers to the values predicted by eqn (2), and *Observed* refers to the values obtained from Tables 2 and 3.

Comparing the data in Tables 2 and 3, one sees that the counting efficiency of the 4-y-old has decreased as this phantom has actually moved away from the detector when in counting geometry 2. With the exception of the reference male phantom and the 95-percentile male phantom, a similar trend is observed for the other phantoms. The reference male phantom is in the same position for both counting geometries, and the 95-percentile male phantom is now closer to the detector in counting geometry 2. The data are also shown in Fig. 5 which presents the ratio of the two counting geometries. This effect is further explored below.

The calibrations have, with the exception of radioiodine, assumed that any nuclide is homogeneously distributed throughout the body following an intake. Often this is not true but it does conform to the calibration methods routinely used by whole body counting facilities throughout the world.

Calibration—thyroid counting

In the special case when a person is contaminated with ^{131}I, the activity will be localized in the thyroid. The relationship of counting efficiency, photon energy, and size (eqn 2) no longer applies as the energy is fixed (365 keV) and weight seems to have little influence. The relation of counting efficiency to phantom height is shown in Fig. 6 for counting geometries 1 and 2. The data were well fitted by the following equation:

$$Z = a + be^{(cY)} + \frac{d}{Y^2}, \qquad (4)$$

where Z = counting efficiency (cnt/photon), Y = phantom height (m), and a to d are regression coefficients.

Table Curve 2D was used to fit the data in Fig. 6. For counting geometry 1, the correlation coefficient was 0.9986, the standard error of the fit was 2.42×10^{-6} and the F-statistic of the fit was 691.9. Similarly, for counting ge-

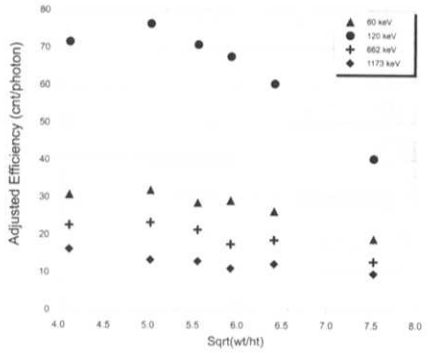

Figure 3. Efficiency multiplied by 10^6 vs. (wt/ht) for selected photon energies (60, 120, 662, 1173 keV) for counting geometry 1. Activity was homogeneously distributed throughout the phantom.

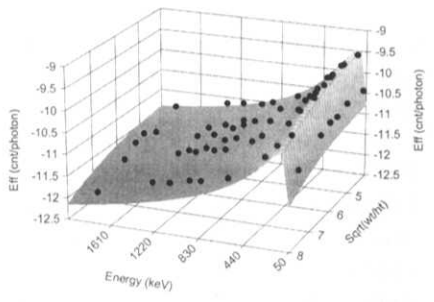

Figure 4. Plot showing the fit of eqn (2) to the data in Table 3 for all of the BOMAB phantoms containing a homogeneous distribution of activity.

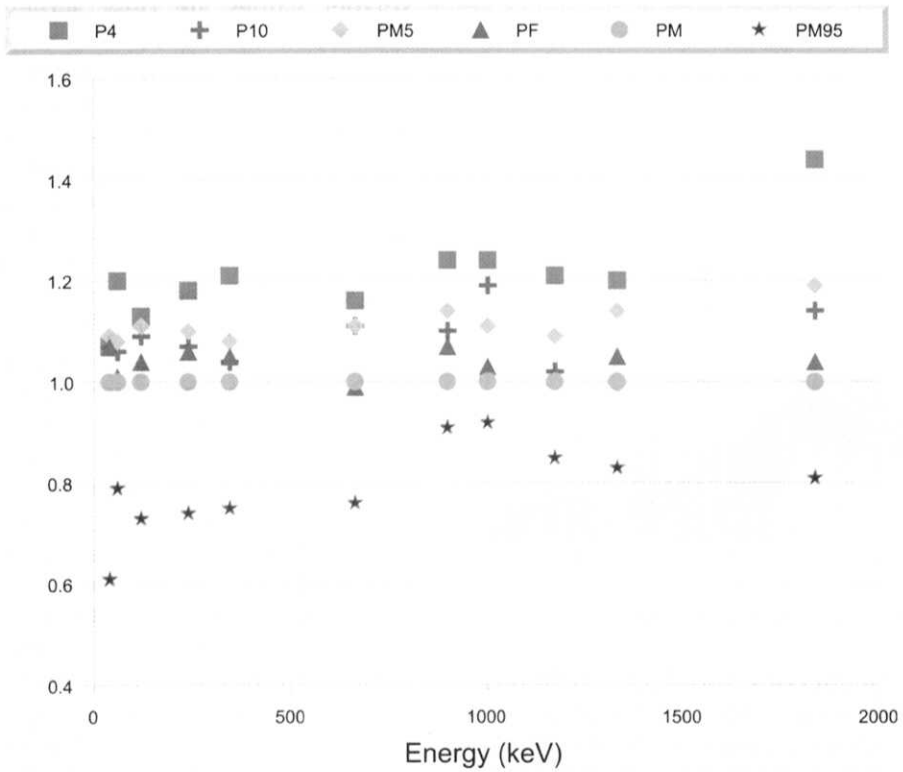

Figure 5. Plot of the ratio of counting efficiencies for a given phantom measured in counting geometry 1 and counting geometry 2 as a function of photon energy (keV).

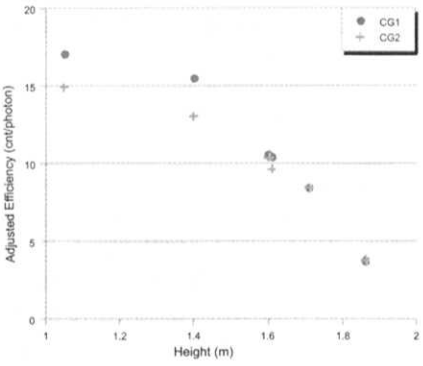

Figure 6. Efficiency multiplied by 10^5 vs. (wt/ht) for 365 keV photons emitted from the neck for counting geometry 1 and counting geometry 2 .

ometry 2 the correlation coefficient was 0.9937, the standard error of the fit was 4.26×10^{-6}, and the F-statistic of the fit was 157.1. Using eqn (4), the efficiency values for both counting geometries in Fig. 6 can be predicted to within 3% (bias) for counting geometry 1 and to within 8% for counting geometry 2. The range of bias (defined in eqn 3) values is from −8 to 5% for both geometries.

The thyroid measurements show the similar trends for the two counting geometries (see Fig. 6) with the counting efficiency apparently decreasing with increasing height. However, the height of the neck for the 4-y-old phantom is below that of the detector whereas all the other phantoms are above it. Thus, there is a height where the neck is level with the detector, and this will give the maximum counting efficiency. This value will lie in between the 4-y-old and 10-y-old phantom data, and eqn (4) predicts this maximum to occur at 1.18 m, which is quite reasonable.

Changing the size of the thyroid gland from 11.0 g to 29.1 g, which covers the range expected of thyroid glands in normal persons (Pankow et a1. 1985), one observes changes in the counting efficiency from 8.45×10^{-5} cnt/photon to 8.99×10^{-5} cnt/photon. These changes do not follow a systematic trend with mass.

The change in counting efficiency represents a maximum variability of 6%. Another way of looking at this result is that the size of a person's thyroid, which is unknown at the time of counting, can introduce an uncertainty into the result on the order of 6%.

Experimental counts

Background. The background spectrum measured in the HML with the Detective is shown in Fig. 7. Photopeaks are present at 238, 352, 511, 584, 610, 911, 969, and 1460 keV. They can be attributed to naturally occurring nuclides that are contained in the building materials of the HML and radon decay products. The radon isotopes (both ^{222}Rn and ^{220}Rn) originate in the HML's sub-basement, which is sand, and are fed into the HML through the local air handling system whose air intake is, ironically, predominantly from that sub-basement. The photopeaks have been identified as ^{212}Pb, ^{214}Pb, annihilation, ^{208}Th, ^{214}Bi, ^{228}Ac, and ^{40}K, respectively.

Regions of the spectrum shown in Fig. 7 corresponding to ^{137}Cs, ^{60}Co, ^{131}1, ^{152}Eu, and ^{241}Am were used to determine the corresponding MDA's for a 5-minute count. The background count data are shown in Table 4 for the energies used for the MDA estimations (60, 344, 365, 660, and 1173 keV).

Disc sources. The results of the initial experimental efficiency determination and the MCNP efficiencies are presented in Table 5 under the subheading of "original design." The adequacy of the model was assessed by examining the ratio of the predicted (MCNP) efficiency to that of the measured efficiency. Table 5 shows that the agreement is good except at the two lowest energies. This suggested that the information provided by the manufacturer was not adequate to accurately model the counting system. Discussing

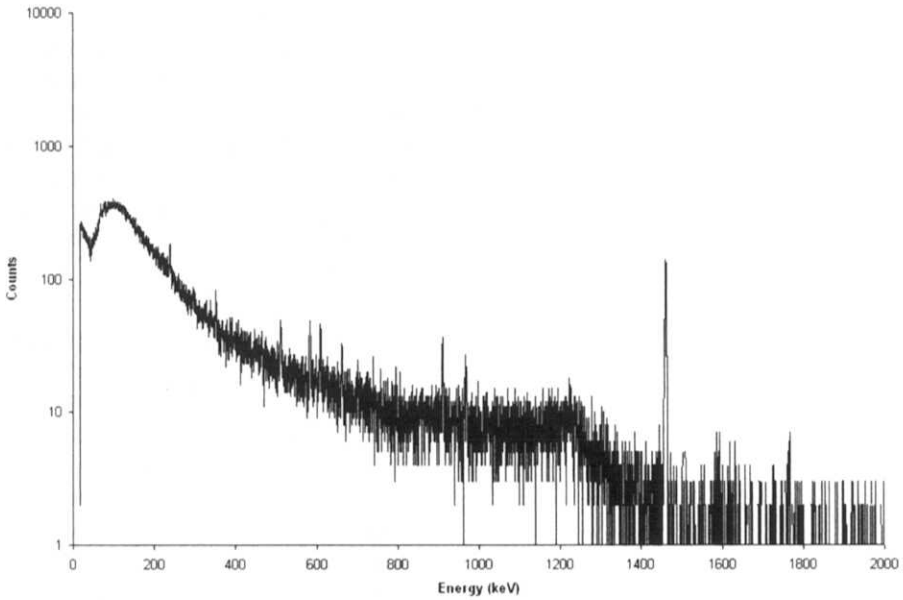

Figure 7. Background spectrum measured in the HML. Count time = 3,600 s.

this finding with the manufacturer, the HML was provided with some more information so that the model could be refined.

Stability of the ratio of the MCNP and measured efficiencies for the disc sources were achieved and the final value, averaged over all energies, was 1.39 ± 0.04 (1σ). This value was used to correct the other counting efficiencies determined from the Monte Carlo simulations (Mallett et al. 1995; RSICC 1997). Normally one would expect this correction factor to be more like 1.13, but these smaller values are only achievable when the model is a close reproduction of the physical model. In this case, our model is cruder than would be preferred because the design of the Detective is proprietary and the model was based on very limited information from the manufacturer and some educated guesswork.

Phantom count. The efficiency values of the 122, 662, 1173, and 1333 keV photopeaks were found to be 5.52×10^{-5}, 1.79×10^{-5}, 1.18×10^{-5}, and 1.18×10^{-5} count/photon, respectively. Comparing these with the predicted values in Table 3 one finds the agreement to be good. Expressed as a bias (obs-predicated)/predicted, the agreement is −8%, −4%, −3%, and 5%, respectively. This clearly shows that the application of the correction factor has adequately transformed the Monte Carlo data into values that are comparable to those obtained experimentally and substantiates previous findings (Mallett et al. 1995; RSICC 1997).

Table 4. Background data used for MDA calculations

Peak energy	ROI start (keV)	ROI stop (keV)	Counts	Count rate (cps)
60	57.3	61.3	2,255	0.6264
344	341.4	345.8	513	0.1425
365	363.0	367.4	443	0.1231
662	658.5	664.2	291	0.0808
1,173	1,169.3	1,175.4	140	0.0389

Count time = 3,600 s.

Table 5. Experimental and MCNP counting efficiencies for disc sources measured at 0.5 m from the end cap of the Detective

Energy (keV)	Efficiency (cnt/photon)	Measured (cnt/photon)	Ratio (MCNP/measured)
Original model design			
60	5.20×10^{-4}	9.41×10^{-5}	5.53
81	5.29×10^{-4}	2.04×10^{-4}	2.59
276	2.59×10^{-4}	1.79×10^{-4}	1.45
303	2.33×10^{-4}	1.53×10^{-4}	1.52
356	1.94×10^{-4}	1.26×10^{-4}	1.54
383	1.82×10^{-4}	1.18×10^{-4}	1.55
662	9.81×10^{-5}	6.40×10^{-5}	1.53
1,173	5.52×10^{-5}	3.64×10^{-5}	1.52
Revised model design			
60	1.35×10^{-4}	9.41×10^{-5}	1.43
81	2.91×10^{-4}	2.04×10^{-4}	1.42
276	2.35×10^{-4}	1.79×10^{-4}	1.31
303	2.12×10^{-4}	1.53×10^{-4}	1.38
356	1.78×10^{-4}	1.26×10^{-4}	1.42
383	1.62×10^{-4}	1.18×10^{-4}	1.37
662	8.78×10^{-5}	6.40×10^{-5}	1.37
1,173	5.17×10^{-5}	3.64×10^{-5}	1.42

Minimum detectable activity (MDA)

MDA values, see Table 6, have been calculated for photon energies of 60, 344, 660, and 1173 keV for the Reference Male BOMAB phantom assuming a homogeneous distribution of the radionuclide and a 5-min count time. Background count rate data were measured experimentally as described above, and the values in Table 4 were combined with the efficiency data in Table 2, which for this phantom are the same as those in Table 3, to obtain the MDA values.

While the results in Table 6 are substantially higher than MDA values that can be obtained in shielded fixed facilities, they are well below the design criterion of 60 kBq. Also, the intent of the field deployable whole body counter is to (a) identify radionuclide mixtures and (b) estimate body bur-

Table 6. MDA values, expressed as kBq, for selected radionuclides for the Reference Male BOMAB phantom

Nuclide	Energy (keV)	Count rate (s^{-1})	MDA (kBq)
^{241}Am	60	0.6264	22.7
^{152}Eu	344	0.1425	12.3
^{131}I	365	0.1231	1.4
^{137}Cs	662	0.0808	4.8
^{60}Co	1,173	0.0389	4.4

Count time = 300 s. The data for ^{131}I assumes it is localized in the thyroid. Values apply to both counting geometry 1 and 2.

dens to quickly assess persons at immediate risk, which this instrument clearly does. The implication of the MDA values is further discussed below.

The MDA for ^{131}I (365 keV) in the thyroid has also been calculated from the data in Table 4 using the efficiency of the Reference Male BOMAB phantom shown in Fig. 6. This result is also well below the criterion of 60 kBq (which is a 0.6 mSv committed effective dose, or a 12.5 mSv committed equivalent dose to the thyroid), showing this instrument to be adequate for thyroid monitoring under the abovementioned conditions.

Dosimetric implications

Assuming that it would take several days to fully deploy the field equipment, one can assign an arbitrary intake of five days prior to a measurement being made for the purpose of assessing the dosimetric implications of the data in Table 3. It will also be assumed that the material is homogeneously distributed throughout the contaminated individual, except of ^{131}1, which is localized in the thyroid gland.

Using the MDA values in Table 6 as a bioassay measurement, one can calculate the intake and, hence, the committed effective dose. The results of these calculations using IMBA are shown in Table 7 with the assumed solubility type of the inhaled material. Judging by ^{241}Am, it is clear that the actinides will cause a problem, and if they are detected in the field other measurement protocols will have to be developed for human monitoring and assessment. Fission and activation products (including ^{131}I), on the other hand, are relatively easy to measure. The committed effec-

Table 7. Intakes corresponding to a body (or thyroid) burden equivalent to the MDA (Table 6) if the intake took place 5 d earlier

Nuclide	Intake (kBq)	Solubility type	Dose value	Units
^{241}Am	248.2	M	6.73	Sv
^{152}Eu	137.3	M	3.74	mSv
^{131}I	1.55	F	0.16	mSv
^{137}Cs	11	F	73.8	μSv
^{60}Co	48.5	M	345	μSv

The solubility type of the material is also included.

Table 8. Ratio of the counting efficiencies of the BOMAB phantoms relative to the reference male (PM) phantom for both counting geometries

			Phantom				
Energy (keV)	P4:PM	P10:PM	PM5:PM	PF:PM	PM95:PM		
			Counting geometry 1			Average	StDev
40	1.30	1.36	1.20	1.21	0.65	1.14	0.28
60	1.17	1.21	1.09	1.11	0.72	1.06	0.20
120	1.18	1.26	1.17	1.12	0.67	1.08	0.23
240	1.26	1.28	1.19	1.16	0.70	1.12	0.24
344	1.33	1.20	1.23	1.14	0.73	1.13	0.23
662	1.21	1.25	1.15	0.94	0.69	1.05	0.23
898	1.26	1.13	1.27	1.08	0.78	1.10	0.20
1,000	1.24	1.17	1.20	1.04	0.79	1.09	0.18
1,173	1.32	1.09	1.06	0.90	0.79	1.03	0.20
1,332	1.35	1.04	1.05	0.87	0.81	1.02	0.21
1,836	1.47	1.11	1.32	1.21	0.74	1.17	0.28
Average	1.28	1.19	1.18	1.07	0.73		
StDev	0.09	0.09	0.08	0.12	0.05		
			Counting geometry 2			Average	StDev
40	1.21	1.27	1.09	1.13	1.07	1.15	0.08
60	0.97	1.15	1.01	1.10	0.91	1.03	0.10
120	1.04	1.16	1.05	1.08	0.91	1.05	0.09
240	1.07	1.19	1.09	1.09	0.95	1.08	0.09
344	1.10	1.16	1.14	1.09	0.98	1.09	0.07
662	1.05	1.12	1.03	0.95	0.90	1.01	0.09
898	1.02	1.03	1.12	1.01	0.86	1.01	0.09
1,000	0.99	0.98	1.07	1.01	0.86	0.98	0.08
1,173	1.09	1.07	0.97	0.89	0.92	0.99	0.09
1,332	1.13	1.04	0.92	0.83	0.97	0.98	0.11
1,836	1.02	0.97	1.11	1.17	0.92	1.04	0.10
Average	1.06	1.10	1.05	1.03	0.93		
StDev	0.07	0.09	0.07	0.11	0.06		

P4 = four-y-old, P10 = ten-y-old, PM5 = five-percentile male, PF = reference female, PM = reference male, PM95 = 95-percentile male. The average ratio (across the energies and across the phantoms) and the standard deviation are also shown.

tive dose resulting from a body burden corresponding to the MDA varies from small to trivial showing that the Detective has sufficient sensitivity to act as a field deployable whole body counter.

Size dependency

The counting efficiency of the phantoms varies with the size. Comparing the other sizes with the reference male phantom provides insight to the variability of field measurements as people come in a wide range of sizes. Table 8 presents the ratios of each phantom's counting efficiency to that of the reference male phantom's counting efficiency for both counting geometries. The data show that counting geometry 1 has larger average ratios for the phantoms than those of counting geometry 2; however, the standard deviation of each set is comparable between the two geometries when averaging over the energies. When averaging over the phantoms at a given energy, the standard deviation for counting geometry 2 is between a factor of two to three smaller than those of counting geometry 1. Counting geometry 2 is, therefore, the preferred geometry as counting efficiency will vary less as a person's size varies.

Future work

The equations developed in this work will be ported to a Visual Basic program that will allow field operatives to quickly estimate body burdens during emergency monitoring when performing in vivo counts in the field.

CONCLUSION

The field deployable Detective can be effectively used as a high resolution whole body counter for fission and activation products. The counting efficiency can be expressed as a function of photon energy and weight and height of the monitored person. This single function allows a wide range of sizes to be adequately measured. In the case of radioiodine, the counting efficiency seems to depend upon height only; a function has been developed that will allow a wide range of heights to be measured with adequate sensitivity.

The overall sensitivity of the portable unit is sufficient for emergency response as it can detect body burdens that will result in a dose that is a few multiples of background or less, depending on the energy of the emitted photons, solubility type, effective half-life, etc.; however, it cannot be used for actinides.

The preferred counting geometry is to place the Detective on a support 1 m above the ground and 70 cm from a wall. Measurement subjects would be placed with their back against the wall and facing the detector. This geometry minimizes the effect of a person's size on the counting efficiency, although it does introduce a slightly higher uncertainty into a thyroid result compared with the other counting geometry that was tested.

REFERENCES

Brodsky A. Accuracy and detection limits for bioassay measurements in radiation protection. Washington, DC: U.S. Nuclear Regulatory Commission; Report NUREG-1156; 1986.

Currie LA. Limits for qualitative detection and quantitative determination: Application to radiochemistry. Anal Chem 40:586–593; 1968.

International Commission on Radiological Protection. Basic anatomical and physiological data for use in radiological protection: reference values. Oxford: Pergamon Press; Publication 89, Annals of the ICRP 32(3/4); 2002.

Kramer GH, Noel L, Burns LC. The BRMD BOMAB family. Health Phys 61:895–902; 1991.

Kramer GH. Increased emergency response activities of the Human Monitoring Laboratory following the tragic events of 11th September, 2001. In: Proceedings of the 11th International Congress of the International Radiation Protection Association, May 23–28. Madrid, Spain: IRPA; 3a19; 2004: 1–2.

Kramer GH, Limson Zamora M. The Canadian National Calibration Reference Centre for Bioassay and In Vivo Monitoring—a program summary. Health Phys 67:192–196; 1994.

Kramer GH, Burns LC, Guerriere S. Monte Carlo simulation of a scanning detector whole body counter and the effect of BOM AB phantom size on the calibration. Health Phys 83:526–533; 2002.

Kramer GH, Capello K. Calibration of the HML's portable whole body counter as a function of BOMAB phantom size and energy modelled by MCNP. Proceedings of the 2004 International Congress on Radiation Protection. Madrid: International Radiation Protection Association; 3a21; 2004.

Mallett MW, Hickman DP, Kruchten DA, Poston Sr JW. Development of a method for calibrating in vivo measurement systems using magnetic resonance imaging and Monte Carlo computations. Health Phys 68:773–785; 1995.

Pankow BG, Michalak J, McGee MK. Adult thyroid weight. Health Phys 49:1057–1103; 1985.

Radiation Safety Information Computational Centre. Computer Code Collection MRIPP 1.0: Magnetic resonance image phantom code system to calibrate in vivo measurement systems. Oak Ridge, TN: Radiation Safety Information Computational Centre; NEA DATA BANK reference MRIPP-CCC-0655/01; 1997.

Smith T, Hesp R, Mackenzie J. Total body potassium calibrations for normal and obese subjects in two types of whole body counter. Phys Med Biol 24:171–175; 1979.

X-5 Monte Carlo Team. MCNP A General Monte Carlo N-Particle Transport Code, Version 5. Los Alamos, NM: Los Alamos National Laboratory; LA-UR-03-1987; 2003.